Check for updates

High sensitivity photonic crystal fiber surface plasmon resonance sensor based on indium tin oxide

Honggang Pan[1] · **Nan Cui**[1] · **Ailing Zhang**[1] · **Yanmei Shi**[1] · **Chuanbo Cao**[1] · **Zhipan Chen**[1] · **Bo Zhang**[1] · **Sihang Lin**[1] · **Guangxiao Cao**[1]

Abstract

In this paper, we propose a high sensitivity photonic crystal fiber surface plasmon resonance sensor based on indium tin oxide (ITO). We select ITO film to improve the sensing performance. According to numerical simulation results, the maximum wavelength sensitivity of the sensor can reach 28,500 nm/RIU. It has the high wavelength resolution of 3.5×10^{-6} RIU and the refractive index detection range is 1.33–1.40. Considering the simple structure and excellent sensing performance, the sensor can detect the refractive index of liquid in a wide range and accurately detect the refractive index of liquid such as blood plasma, hemoglobin, etc.

✉ Yanmei Shi
zjh022@126.com

✉ Bo Zhang
zhb.q@icloud.com

Honggang Pan
phg022@email.tjut.edu.cn

Nan Cui
cuinan19990118@163.com

Ailing Zhang
alzhang@email.tjut.edu.cn

Chuanbo Cao
875335537@qq.com

Zhipan Chen
zhipanchen@163.com

Sihang Lin
1750229649@qq.com

Guangxiao Cao
1076225823@qq.com

1 Engineering Research Center of Communication Devices and Technology, Ministry of Education, Tianjin Key Laboratory of Film Electronic and Communication Devices, School of Integrated Circuit Science and Engineering, Tianjin University of Technology, Tianjin 300384, China

1 Introduction

In the past decades, there has been a great interest in the design of artificial micro nano structure devices, such as absorbers (Qin et al. 2020), lenses (Zhao et al. 2020), logic gates (Ge et al. 2020), topological waveguide devices (Hou et al. 2020) and biosensors (Wang et al. 2019) et al. Among these optical devices, surface plasmon resonance (SPR) sensors are widely used in environmental monitoring, biochemical analysis, etc. Although the Kretschmann-Raether structure was proposed in 1968 to excite the SPR effect, the disadvantages of its structure, such as the large size, limit the miniaturization of the sensor (Kretschmann and Raether 1968). After the concept of photonic crystal being proposed in 1987, photonic crystal fiber (PCF) gradually entered the vision of scientists. Due to its good transmission characteristics, researchers applied PCF to SPR sensor (Bender and Dessy 1994; Liu and Wang 2020).

Currently, two kinds of design methods have been proposed based on PCF-SPR sensors: one is internal sensing and the other is external sensing (Ramani and Kumar 2021). In terms of internal sensing, in 2020, Liu and Ma (2020). However, the internal sensing technology requires liquid penetration and selective metal coating, the structure and manufacturing process are both complex (Haider et al. 2018). A simpler method is external sensing which directly coating a film of material on the outer surface of the PCF. In 2019, Liu et al. (2019a, b). proposed an eccentric nuclear photonic quasicrystal fiber (PQF) sensor based on SPR with a sensitivity of 21,000 nm/RIU and in 2020, Nashaye Rafi et al. (2020). proposed a PCF sensor based on SPR with a sensitivity of 8000 nm/RIU. However, their structures are complex and their sensitivities are relatively low.

The performance of SPR sensors is highly depend on the conductor material of the plasma layer used in the sensor. Conductor material of the plasma layer is commonly silver or gold. Compared with gold and silver, indium tin oxide (ITO) is a cheaper and better conductor. ITO also has adjustable photoelectric properties and low loss in the infrared range. So we adopted ITO as the conductor material. In 2020, Chao Liu et al. designed an ITO SPR sensor with a sensitivity of 15,000 nm/RIU(Liu 2020). But its sensitivity is relatively low. The sensitivity of the sensor described above can be improved greatly and the structure can be simplified.

In this paper, a high sensitivity photonic crystal fiber (PCF) surface plasmon resonance sensor based on indium tin oxide (ITO) is proposed. By using single air hole size type, the sensor structure is greatly simplified with only four air holes which are easy to manufacture. By optimizing the sensor structure parameters, it can achieve high sensitivity of 28,500 nm/RIU, resolution of 3.5×10^{-6} RIU and the refractive index detection range of the sensor is 1.33–1.40. Our proposed sensor can be widely used in chemical and medical fields.

2 Structural design and theoretical modeling

The cross-section model of the proposed sensor is shown in Fig. 1a. We choose fused silica as the background material. Inside the perfect matching layer (PML) is the analyte layer whose thickness is 3.5 μm and the thickness of the PML is 1.5 μm which is used to absorb radiation energy (Islam et al. 2019). The thickness of the ITO film is t.
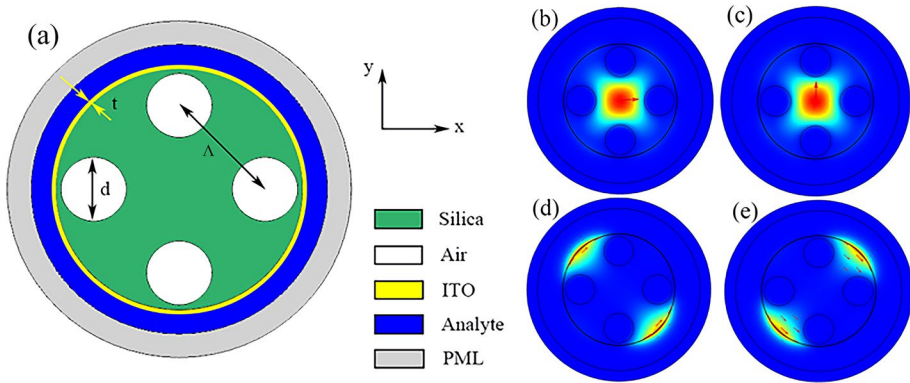
Fig. 1 **a** The cross section of the proposed sensor; **b–c** The fundamental mode light field diagram of x-pol and y-pol when RI = 1.39; **d-e** the SPP mode light field diagram of x-pol and y-pol when RI = 1.39.

In the coverage area of the background material, there are four air holes with diameter of d which arranged in a square and the distance between air holes is Λ. Figure 1b-e show light field diagram of the fundamental mode and SPP mode in the two polarization modes.

The dispersion relationship of the proposed sensor with the refractive index of 1.39 is shown in Fig. 2. It can be seen from Fig. 2 that the resonance wavelengths of two polarization modes are both at 1865 nm. Because the structure is symmetrical, the mode fields and loss spectrum are similar for both polarization modes. Therefore, in the subsequent parameter optimization process, the y-polarization mode of the structure is selected for analysis. It can be seen from Fig. 2 when the incident wavelength is shorter than the resonance wavelength, the energy of the fundamental mode is well confined in the fiber core. As the wavelength of the incident light increases, the fundamental mode gradually couples with the SPP mode. There is a sudden change in $Re(n_{eff})$ for both modes when the wavelength reaches the resonance wavelength, the energy of the fiber core transferred to the SPP mode.

The dispersion relationship of the fused silica is calculated by Sellmeier equation (Soghra et al. 2022):
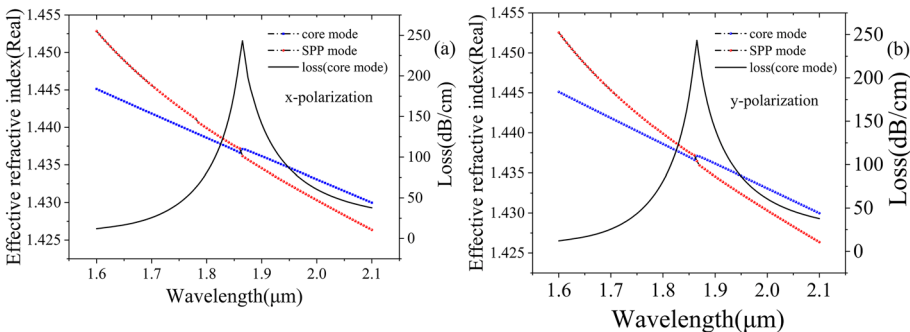

Fig. 2 **a–b** Dispersion relation of the fundamental mode, SPP mode, and confinement loss spectrum when n = 1.39, d = 4.1 μm, Λ = 7.6 μm and t = 50 nm

$$n^2(\lambda) = 1 + \frac{B_1\lambda^2}{\lambda^2 - C_1} + \frac{B_2\lambda^2}{\lambda^2 - C_2} + \frac{B_3\lambda^2}{\lambda^2 - C_3} \tag{1}$$

In this expression, B_1, B_2, B_3, C_1, C_2 and C_3 are 0.6961663, 0.4079426, 0897479400, 0.0046791486, 0.0135120631 and 97.9340025, respectively. Here, λ is the incident light wavelength in vacuum.

The dielectric constant of ITO is expressed by Eq. 2 (Liu et al. 2019a, b):

$$\varepsilon_m(\lambda) = \varepsilon_\infty - \frac{\lambda^2\lambda_c}{\lambda_p^2(\lambda_c + i\lambda)} \tag{2}$$

In this expression, $\lambda p = 5.6497 \times 10^{-7}$ m and $\lambda c = 11.21076 \times 10^{-6}$ m are the plasmonic wavelength and collision wavelength of ITO, respectively, $\varepsilon_\infty = 3.80$ is the dielectric constant for the infinite value of the frequency of ITO, and λ is the operating wavelength in micron.

The confinement loss of this sensor can be expressed by Eq. 3 (Wang and Li 2019):

$$Loss(dB/cm) = 8.686 \times k_0 \times \text{Im}(n_{eff}) \times 10^4 \tag{3}$$

In this expression, $k_0 = 2\pi/\lambda$ is the wave number, λ is in micron. $\text{Im}[n_{eff}]$ is the imaginary part of the effective refractive index.

The sensitivity of this sensor can be expressed by Eq. 4 (Aslam Mollah and Islam 2020):

$$S_\lambda(nm/RIU) = \frac{\Delta\lambda_{peak}}{\Delta n} \tag{4}$$

In this expression, $\Delta\lambda_{peak}$ is resonance peak offset, Δn is the refractive index variation value.

The resolution is this sensor can be expressed by Eq. 5 (Wang et al. 2021):

$$R(RIU) = \Delta n \frac{\Delta\lambda_{\min}}{\Delta\lambda_{peak}} \tag{5}$$

In this expression, $\Delta\lambda_{min}$ represents the offset of the wavelength.

3 Results and discussion

In order to improve the sensing performance, we systematically studied the influence of structural parameters on the loss spectrum. The following analysis of structural parameters was performed at the analyte refractive index of 1.39 and 1.40.

Figure 3 shows the loss spectrum of different air hole diameters when the refractive index are 1.39 and 1.40 with the air hole spacing $\Lambda = 7.4$ μm and the thickness of the ITO layer t = 50 nm.

It can be seen from Fig. 3 that with the increase of the air hole diameter, the loss spectrum is red-shifted and the peak value of the loss spectrum gradually decreases. Because increasing the diameter of the air hole can better restrict the transmission of light in the fiber core, the light leaking to the ITO layer is reduced. The peak value of the loss spectrum decreases. When the air hole diameter is 4.0 μm, 4.1 and 4.2 μm, the sensitivities are 18,500 nm/RIU, 19,500 nm/RIU and 20,000 nm/RIU at the refractive index changes from

Fig. 3 Loss spectrum of different air hole diameters at RI = 1.39 and RI = 1.40.
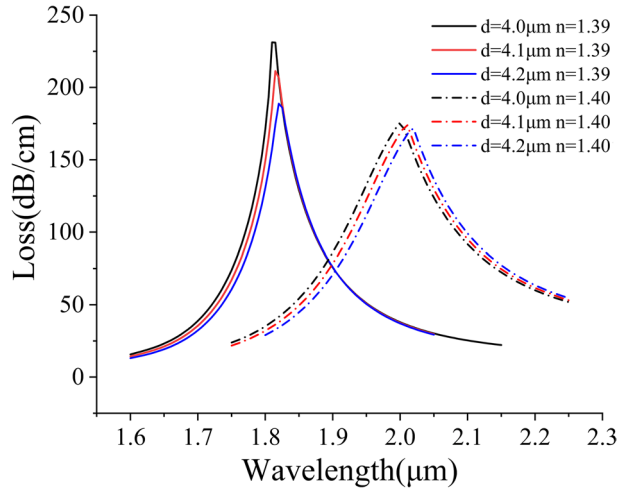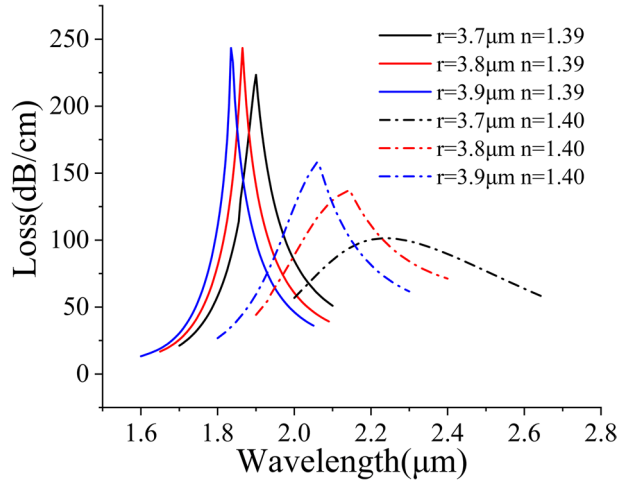

Fig. 4 Loss spectrum of different air hole spacing at RI = 1.39 and RI = 1.40.

1.39 to 1.40, respectively. However when the air hole diameter is 4.2 μm, the peak value of loss spectrum is relatively low. Therefore, the optimal parameter of the air hole diameter d is 4.1 μm. The air hole spacing Λ also has great influence on sensor performance. Figure 4 shows the loss spectra of the air hole spacing Λ of different parameters at refractive index 1.39 and 1.40 when the air hole diameter d = 4.1 μm and thickness t = 50 nm of ITO layer. It can be seen from Fig. 4 that the loss spectrum is blue-shifted with the increase of the air hole spacing Λ and the peak of the loss spectrum gradually increases. Moreover, the peak value of the loss spectrum increases because enlarging the air hole spacing will make more light leakage into the ITO layer.

It can be seen from Fig. 4 that when the air hole spacing Λ = 7.4 μm, the loss spectrum has no obvious peak under the condition of the refractive index of 1.40 which severely affects sensor performance. The air hole spacing Λ = 7.6 μm is similar to the peak of the loss spectrum of the air hole spacing Λ = 7.8μm. But the sensitivity of 28500 nm/RIU when the air hole spacing Λ = 7.6 μm is higher than that the sensitivity

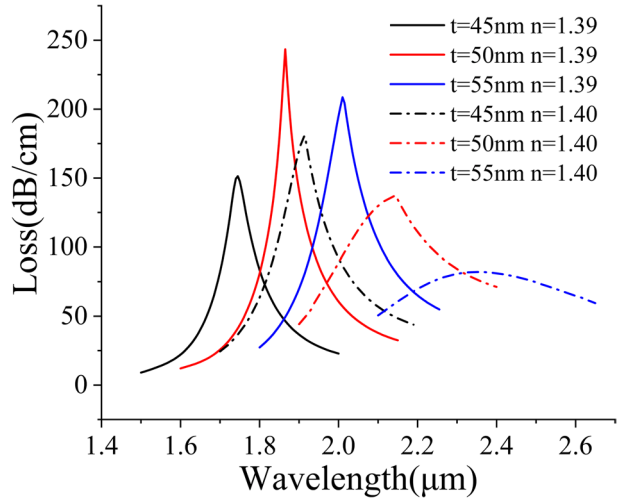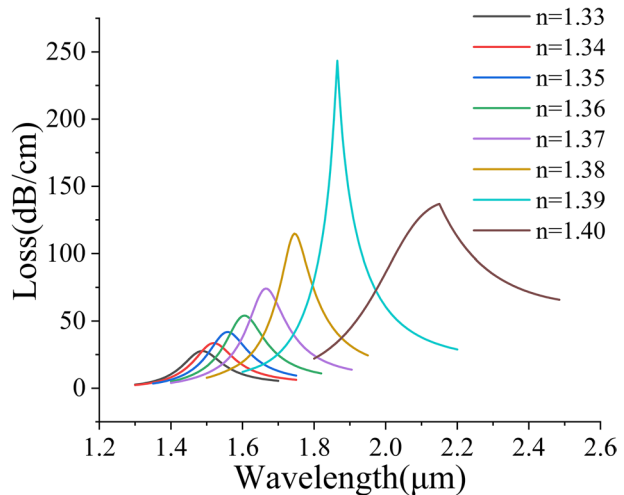**Fig. 5** Loss spectrum of ITO layer of different thickness at RI of 1.39 and 1.40

Fig. 6 Loss curves of the proposed sensor for different analyte RI (1.33–1.40)

of 22500 nm/RIU when the air hole spacing $\Lambda = 7.8$ μm. Therefore, we choose the air hole spacing $\Lambda = 7.6$ μm as the optimal size.

It can be seen from Fig. 5 that the peak of the loss spectrum is the highest when the thickness $t = 50$ nm of the ITO layer. Although the sensor sensitivity is greater at the thickness $t = 55$ nm of the ITO layer, the full width at half maximum (FWHM) of the loss spectrum is too large when the refractive index is 1.40. Therefore, the thickness $t = 50$ nm of the ITO layer is the optimal size.

The excitation of the SPP mode mainly depends on the ITO layer and the thickness of the ITO layer also has a significant impact on the performance of the sensor. If the thickness of the ITO layer is too large, the electric field does not easily break down the ITO layer, resulting in a decrease the peak of the loss spectrum. If the ITO layer is too thin, the surface plasma wave will be strongly damped because of radiation damping.

Table 1 The performance of the proposed sensor

Refractive index	Resonance wavelength (nm)	Sensitivity (nm/RIU)
1.33	1490	N/A
1.34	1520	3000
1.35	1560	4000
1.36	1605	4500
1.37	1665	6000
1.38	1745	8000
1.39	1865	12,000
1.40	2150	28,500

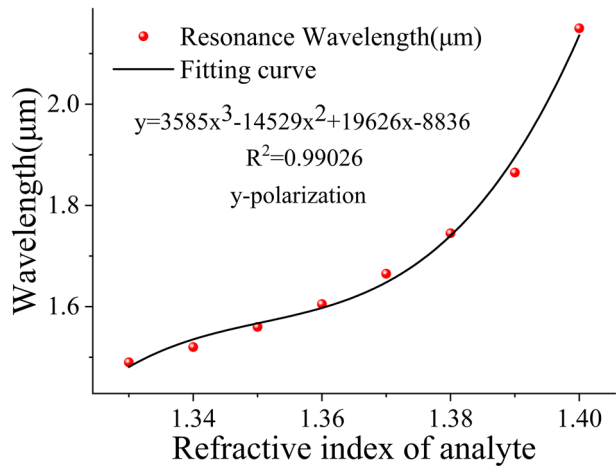**Fig. 7** Variation of resonance wavelength with analyte RI and fitting curve

Figure 6 shows the loss spectrum of the proposed sensor with the different refractive index. It can be seen from Fig. 6 that the loss spectrum is red-shifted with the increase of the refractive index. When the refractive index increases, the real part of the effective refractive index of the SPP mode increases, while the real part of the effective refractive index of the fundamental mode does not change, which results in red shifting of the loss spectrum. The maximum value of the loss spectrum is 243.42 dB/cm when the refractive index n = 1.39. The change of sensitivity with refractive index is shown in Table 1. The sensitivity and resolution of the sensor are calculated by Eqs. 4 and 5, respectively. The sensitivity is 28,500 nm/RIU when the refractive index is 1.39–1.40 and the sensor resolution is 3.5×10^{-6} RIU. It can be seen that the sensor's refractive index detection range is 1.33–1.40.

Figure 7 is the fitting curve for variation of resonance wavelength with analyte RI. The fitting coefficient is $R^2 = 0.99026$. Table 2 shows the performance of our proposed sensor compared with other sensors, it can be seen that our sensor has achieved the high sensitivity and the structure is simple.

Table 2 Performance comparison with similar sensors

References	Refractive index range	Maximum sensitivity (nm/RIU)	Air holes number
Liu (2020)	1.33–1.39	8000	17
Liu and Sun (2020)	1.33–1.39	21,000	17
Hossaina and Hossain (2020)	1.42–1.46	15,000	36
Chao Liua and Fua (2019)	1.33–1.40	14,200	16
Kaur and Singh (2019)	1.385-1.40	10,000	19
This paper	1.33–1.40	28,500	4

4 Conclusion

In this paper, we propose a high sensitivity photonic crystal fiber (PCF) surface plasmon resonance sensor based on indium tin oxide (ITO). The highest sensitivity is 28,500 nm/RIU and the resolution is 3.5×10^{-6} RIU. The sensor has a refractive index detection range of 1.33–1.40, which includes various chemical solutions and biochemicals, such as red blood cells (1.40), white blood cells (1.36), human intestinal mucosa (1.329–1.338), 10% glucose solution (1.3477), acetone (1.36), human liver (1.369) (Wang and Li 2019), etc. The sensor achieves high-sensitivity detection of the analyte, and the simple structure also provides more feasibility for practical fabrication.

Data availability Any datasets in this manuscript are owned by the authors, and the authors may be contacted to request any data used in the manuscript if required.

Declarations

Conflict of interest The authors declare that they have no known competing financial interests or personal relationships that could have appeared to influence the work reported in this paper.

Ethical approval For this manuscript, the declaration of ethical approval is not applicable.

References

Aslam Mollah, M., Saiful Islam, M.: Novel single hole exposed-suspended core localized surface plasmon resonance sensor. IEEE Sens. J. **21**(3), 2813–2820 (2021)

Bender, W.J., Dessy, R.E.: Surface plasmon resonance sensor, Google Patents. 237–248 (1994)

Ge, R., Yan, B., Xie, J., Liu, E., Tan, W., Liu, J.: Logic gates based on edge states in gyromagnetic photonic crystal. Magn. Mater. **500**, 166367 (2020)

Haider, F., Ahmmed Aoni, R., Ahmed, R., Islam, S., Miroshnichenko, E.: Propagation controlled photonic crystal fiber based plasmonic sensor via scaled-down approach. IEEE Sens. J. 962–969 (2018)

Hossaina, B., Hossain, S.: Numerical development of high performance quasi D-shape PCF-SPR biosensor: an external sensing approach employing gold. Results Phys. **18**, 103281 (2020)

Hou, T., Ge, R., Tan, W., Liu, J.: One-way rotating state of multi-periodicity frequency bands in circular photonic crystal. Phys. D Appl. Phys. **53**(7), 075104 (2020)

Islam, S., Cordelro, C.M.B., Sultana, J.: A Hi-Bi ultra-sensitive surface plasmon resonance fiber sensor. Digit. Object Identifier **1109**, 79085–79094 (2019)

Kaur, V., Singh, S.: Design of titanium nitride coated PCF-SPR sensor for liquid sensing applications. Opt. Fiber Technol. **48**, 159–164 (2019)

Kretschmann E, Raether H.: Notizen: radiative decay of non radia-tive surface plasmons excited by light. Z Naturforschung **23**(12), 2135–2136 (1968)

Liu, Q., Sun, J.: Surface plasmon resonance sensor based on photonic crystal fiber with indium tin oxide film. Optic. Mater. **102**, 109800 (2020)

Liu, Q., Ma, Z.: The biochemical sensor based on liquid-core photonic crystal fiber filled with gold, silver and aluminum. Opt. Laser Technol. **130**, 106363 (2020)

Liu, Q., Sun, J.: Surface plasmon resonance sensor based on eccentric core photonic quasi-crystal fiber with indium tin oxide. Opt. Mater. **102**, 109800 (2020)

Liu, C., Wang, J.: Surface plasmon resonance (SPR) infrared sensor based on D-shape photonic crystal fibers with ITO coatings. Opt. Commun. **464**, 125496 (2020)

Liu, Q., Sun, J., Sun, Y., Liu, W., Wang, F., Yang, L., Liu, C., Liu, Q., Li, Q., Ren, Z., Sun, T., Chu, P.K.: Surface plasmon resonance sensor based on eccentric core photonic quasi-crystal fiber with indium tin oxide. Appl. Opt. **58**(25), 6848–6853 (2019)

Liu, Q., Jiang, Y., Sun, Y.: Surface plasmon resonance sensor based on U-shaped photonic quasi-crystal fiber. Appl. Opt. 1761–1766 (2019b)

Liua, C., Fua, G.: Ex-centric core photonic crystal fiber sensor with gold nanowires based on surface plasmon resonance. Optik **196**, 163173 (2019)

Nashaye Rafi, H., Rejvi Kaysir, M., Jahirul, M., Islam: Air-hole attributed performance of photonic crystal fiber-based SPR sensors. Sens. Bio-Sens. Res. **29**, 100364 (2020)

Qin, F., Chen, Z., Chen, X., Yi, Z., Yao, W., Duan, T., Wu, P., Yang, H., Li, G., Yi, Y. A tunable triple-band near-infrared metamaterial absorber based on au nanocuboids array, Nanomater **10**(2), 207 (2020)

Ramani, U., Kumar, H. Design of surface plasmon resonance based both side polished photonic crystal fiber for highly efficient refractive index sensor, Optik **248**, 168062 (2021)

Soghra, G., Jamal, B., Bahar, M. Design and analysis of surface plasmon resonance based photonic crystal fiber sensor employing gold nanowires, Optik **260**, 169026 (2022)

Wang, S., Li, S.: Surface plasmon resonance sensor based on symmetrical side-polished dualcore photonic crystal fiber. Opt. Fiber Technol. **51**, 96–100 (2019)

Wang, X., Zhu, J., Wen, X., Wu, X., Wu, Y., Su, Y., Tong, H., Qi, Y., Yang, H. Wide range refractive index sensor based on a coupled structure of au nanocubes and au film, Opt. Mater. Express **9**(7), 3079–3088 (2019)

Wang, Y., Li, S., Wang, M.: A high-sensitivity refractive index sensor based on an external gold coating of a square-lattice photonic crystal fiber. Phys. Status Solidi RRL **15**, 2100001 (2021)

Zhao, H., Xie, J., Liu, J.: An approximate theoretical explanation for super-resolution imaging of two-dimensional photonic quasi-crystal flat lens. APEX **13**(2), 022007 (2020)